Conference paper

Vladimír Zeleňák*, Jozef Magura, Adriána Zeleňáková and Romana Smolková

Carbon dioxide and methane adsorption over metal modified mesoporous SBA-15 silica

DOI 10.1515/pac-2016-1121

Abstract: In the present study, mesoporous silica materials doped with metal ions (Al^{3+}, Ti^{4+}, Zr^{4+}) were synthesized and characterized by a combination of various techniques, such as small angle X-ray scattering (SAXS), nitrogen adsorption/desorption at 77 K, elemental analysis, transmission electron microscopy (HRTEM) and scanning electron microscopy (SEM). It was shown that the metal ion doped samples retained their porous structure, which was similar to that of parent SBA-15. The synthesized M-SBA-15 samples (M = Al^{3+}, Ti^{4+}, Zr^{4+}) were evaluated in terms of adsorption of carbon dioxide and methane at 303 K. It was observed, that metal doping enhances carbon dioxide adsorption in comparison with purely siliceous sample, while low effect of metal doping on methane adsorption was observed.

Keywords: carbon dioxide; mesoporous silica; metal doping; methane; SBA-15; SSC-2016.

Introduction

Ordered mesoporous silicas were first reported in 1992 when Mobil Oil Company developed mesoporous silica material MCM-41 [1]. This discovery was followed by the development of other ordered mesoporous silica materials such as SBA family (Santa Barbara Amorphous type materials), FDU (Fudan University Material), KIT (Korea Advanced Institute of Science and Technology) and others. Since 1990s, significant progress has been made in control of their structure and pore size, composition variation and applications [2]. One of the most important milestones in preparation of mesoporous materials was synthesis of thick-walled hexagonally ordered SBA-15 silica with high hydrothermal stability [3]. However, this material has weak reactivity of silica surface caused by silanol groups, which are only able of formation of hydrogen bonds with guest gaseous molecules, and which are insufficiently ionized in aqueous solutions. This lack of surface reactivity can be overcome by functionalization of silica materials with heteroatoms such as Ti, Zr, Al. Generally, there are two methods leading to metal doped silica materials: direct synthesis and post-synthesis functionalization. Direct synthesis allows insertion of heteroatoms straight into the silica framework while maintaining large surface area with narrow pore size distribution. The different sizes of

Article note: A collection of invited papers based on presentations at the 12th Conference on Solid State Chemistry (SSC-2016), Prague, Czech Republic, 18–23 September 2016.

***Corresponding author: Vladimír Zeleňák,** Department of Inorganic Chemistry, Faculty of Science, P.J. Šafárik University, Moyzesova 11, 04154 Košice, Slovakia, e-mail: vladimir.zelenak@upjs.sk
Jozef Magura and Romana Smolková: Department of Inorganic Chemistry, Faculty of Science, P.J. Šafárik University, Moyzesova 11, 04154 Košice, Slovakia
Adriána Zeleňáková: Department of Solid State Physics, Faculty of Science, P.J. Šafárik University, Park Angelinum 9, 04154 Košice, Slovakia

[MO_4] tetrahedral units, caused by increasing M–O bond lengths in the order Si < Al < Ti < Zr, often cause local deformation of inorganic framework assembled around templating micellar structures. The mechanism of [MO_4] and [SiO_4] condensation is very dependent on experimental conditions. In case of materials based on SBA-15, the main difficulty is low stability of M–O–Si bonds under strongly acidic hydrothermal conditions [4–6].

Lin et al. reported direct synthesis of Al-SBA-15 with tuneable aluminosilicate structures in an acid-free medium. The high stability was reported for these mesoporous materials as a result of presence of the plug structures inside the straight channels that are resistant to steaming and alkali post-treatments [7]. Similarly, incorporation of metals into the siliceous structure can also stabilize titania and zirconia materials. Titania and zirconia mesostructures have weak thermal stability and the calcination of these materials often results in poorly ordered or even collapsed mesostructures. Thus, an effective way to eliminate the stability problems is an insertion of titania and zirconia into mesoporous silica [8]. Ti or Zr doped ordered mesoporous SBA-15 materials possess a high surface area even at high TiO_2 or ZrO_2 amounts and furthermore they possess more surface hydroxyl groups than pure titania or zirconia [9].

Many studies have shown that Al, Ti or Zr incorporated silicas can be successfully used as heterogenous catalysts in various organic reactions among which transesterification, cracking and oligomerization have recently triggered an interest in the research fields. Liang et al. used ordered mesoporous Al-SBA-15, prepared by direct synthesis as a support for transesterification of canola oil to produce biodiesel. The study showed, that mesopore and surface acidity provides a significant improvement in transesterification activity due to the formation of stable ≡Si–O–Al≡ bonds [10]. Mouli et al. prepared different heteroatom (Ti, Zr, and TiZr) doped SBA-15 as supports for NiMo catalysts. Hydrodesulfurization and hydrodenitrogenation conversions of the light gas oil were carried out in catalytic experiments. The choice of the heteroatom significantly influenced the molybdenum phase of the catalysts which considerably affected the final catalysis [11].

Chen et al. [12] reported Ti-SBA-15 material obtained by direct synthesis (co-condensation method) which was shown to be an efficient and reusable solid acid catalyst for high quality biodiesel fuel production, through transesterification of various vegetable oils with methanol. Ti-SBA-15 was significantly more efficient and water more tolerant than conventional TiO_2 catalyst. Melero et al. recently reported a synthetic method for the preparation of Zr-SBA-15 materials based on a direct synthesis procedure using zirconocene dichloride as precursor. Zr-SBA-15 exhibited high stability, reusability and catalytic activity in fatty acid methyl esters production by methanolysis of highly acidic crude palm oil [13, 14].

Mesoporous materials are also very promising as molecular sieves for adsorption of different gases. Han et al. prepared different Ti-SBA-15 materials and investigated impact of Ti doping content on the adsorption capacity of hydrogen. The results showed that increasing Ti/Si molar ratio increased amount of titanol and bridging hydroxyl groups and decreased hydrogen adsorption capacity. The best hydrogen adsorption capacity showed Ti-SBA-15 material with Ti/Si molar ratio of 0.1 [15].

Metal doped mesoporous silicas were also investigated as a sorbents of carbon dioxide as a greenhouse gas. Zukal et al. [16] reported, that he doping of Al-SBA-15 with sodium or potassium cations dramatically enhances adsorption in the region of equilibrium pressures lower than 10 kPa and aluminosilicate adsorbents doped with Na^+ or K^+ cations are suitable for carbon dioxide separation from dilute gas mixtures. Zhao et al. [17] reported, that Ti-SBA-15 showed a particularly high CO_2 adsorption capacity of 1.44 $mmol \cdot g^{-1}$, and titanium played an important role in the CO_2 adsorption.

In our previous works we have shown that amine modified nanoporous silica materials have high affinity to carbon dioxide and they can be used for separation of carbon dioxide especially at low partial pressures of CO_2 [18–20]. As a follow up work we investigated the properties of nanoporous silica modified by different metal ions. The gas adsorption can be affected by the nature of gas-solid interactions. The strength of intermolecular forces in gas-solid interface depends on the polarizability of gaseous molecules and the charge density of active sites on the solid surface. Since the charge densities of the metal ions are determined by their ionic radius and the charge, we were interested in influence of modification of SBA-15 silica by the different metal ions (Al^{3+}, Ti^{4+} and Zr^{4+}) on sorption properties of the materials.

Experimental

Synthesis of materials

Mesoporous silica SBA-15 was synthesized by conventional procedure using triblock copolymer Pluronic P123 ($(EO)_{20}(PO)_{70}(EO)_{20}$) and tetraethylortosilicate ($Si(OC_2H_5)_4$, TEOS) in acidic conditions (HCl) [3]. A typical gel composition in terms of molar ration was TEOS/HCl/H_2O/P123 = 1/5.9/193/0.017. A portion of 4.0 g of Pluronic P-123 was dissolved with stirring in a mixture of 30 g of water and 120 g of 2 M HCl at 35 °C and 8.5 g of TEOS was added after dissolution. The resulting mixture was stirred at 35 °C for 20 h and then was aged at 80 °C for 24 h. The as-synthesized sample was recovered by filtration and freely dried. The organic template was removed by calcination in air at 500 °C for 7 h.

For the preparation of metal doped samples a modified procedure reported in [11] was applied. The titanium(IV)-isopropoxide $Ti(OC_3H_7)_4$, aluminium(III)-isopropoxide $Al(OC_3H_7)_3$ and zirconium-tert-butoxide $Zr(OC(CH_3)_3)_4$ were used as metal sources in the synthesis. In a typical synthesis, 8.5 g of TEOS, the required amount of the respective metal alkoxide to maintain Si/M molar ratio = 25 (M = Al, Ti or Zr) and 2g of water were mixed and stirred for 1 h at 20 °C. After this time, the mixture was added to the HCl solution of Pluronic P123. The final synthesis gel had the molar ratio Si/M/HCl/H_2O/P123 = 1/0.04/5.9/193/0.017 (M = Al, Ti or Zr). The resulting mixture was stirred for 24 h at 30 °C, then transferred to the teflon lined steel autoclave and kept at 80 °C for 24 h. The solid product was recovered by filtration, washed with water several times, and dried overnight. Finally, the product was calcined at 500 °C to remove the template.

Characterization

The small angle X-ray scattering (SAXS) experiments were carried out at B1 Hasylab/Desy beamline with the beam energy 12 keV ($\lambda = 1.03$ Å) using PILATUS detector. The HRTEM micrographs were taken with a JEOL JEM 3010 (LaB_6 cathode) microscope operated at 300 kV. Copper grid coated with a holey carbon support film was used to prepare samples for the TEM observation. A powdered sample was dispersed in ethanol and the suspension was treated in an ultrasonic bath for 10 min. Scanning electron micrographs were measured on Tescan Vega instrument. Quantitative estimation of Si/M ratio in the samples was performed using inductively coupled plasma mass spectrometer (Agilent). The samples were digested by acid treatment with H_2SO_4 and HF. The porosity and specific surface area of materials were determined at 77 K by nitrogen adsorption/desorption using Quantachrome NOVA 1200e surface area and pore size analyser. Prior to the experiments, the samples were outgassed at 423 K for 24 h. To confirm reproductivity of measurements and suitability of selected temperature of activation, the control measurements for new batch of the sample and higher temperature of activation (473 K) were performed. Original and control measurements were similar, confirming homogenous dispersion of metal ions in the samples and sufficiency of temperature 423 K selected for degassing. The specific surface area, S_{BET}, was estimated using the Brunauer-Emmett-Teller (BET) equation in a pressure range 0.05–0.30. Pore size distribution was calculated using the NLDFT method as well as Barrett, Joyner and Halenda (BJH) method. Carbon dioxide and methane adsorption isotherms were measured at 303 K by commercial gravimetric equipment IGA001 (Hiden Isochema) using sample weight 50 mg. Prior the measurements the sample were degassed under vacuum at 250 °C for 8 h.

Results and discussion

TEM, SEM characterisation and elemental analysis

The periodic structure of the samples was confirmed by HRTEM measurements. The HRTEM micrographs of the M-SBA-15 samples (M = Al, Ti, Zr) (see Fig. 1) show on periodic hexagonal well-organized mesostructures,

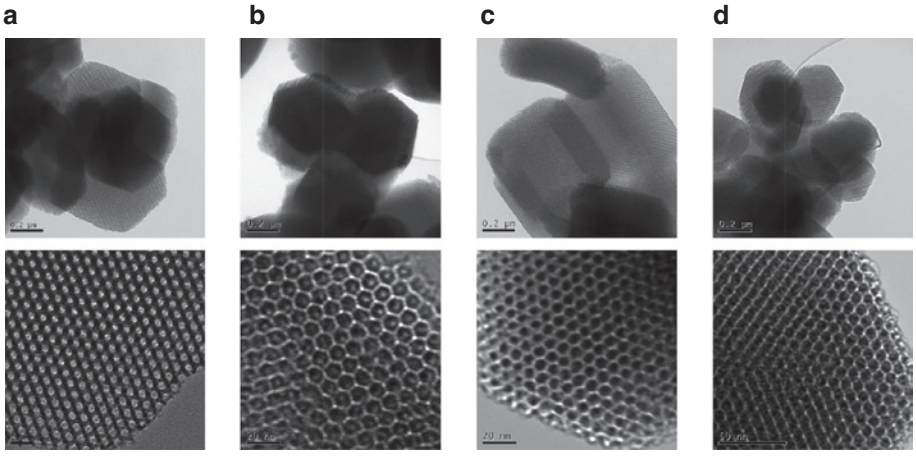

Fig. 1: HRTEM micrographs of the samples SBA-15 (a), Al-SBA15 (b), Ti-SBA15 (c), Zr-SBA15 (d).

formed by alternating pores and silica walls. The unit cell parameter of the hexagonal mesostructures, as estimated from HRTEM micrographs, is about 8 nm for SBA-15, 9 nm for Al-SBA-15 and Ti-SBA-15 and 10 nm for Zr-SBA-15. These values are in a good agreement with the values calculated from SAXS and nitrogen adsorption data (see below). The ICP-MS measurements confirmed experimental Si/M molar ratio 23.5 (M = Al), 26.3 (M = Ti) and 26.7 (M = Zr).

The scanning electron micrographs (SEM) of the prepared materials show, that morphology of all prepared samples is quite similar and samples consist of uniformly sized particles of glomerular appearance (see Fig. 2). The average particle size determined from SEM micrographs is about 720 × 180 nm.

SAXS characterisation

Figure 3a shows the SAXS patterns of pure siliceous SBA-15 and samples modified with Al^{3+}, Ti^{4+} and Zr^{4+} ions. For all materials a diffraction peaks indexed as (10), (11), and (20) in the hexagonal *P6mm* symmetry can be observed. It is obvious that (10) diffraction peak shifts to lower *q* values after modification of SBA-15 silica by metals and the respective *q* values were observed at 0.0658 $Å^{-1}$ for SBA-15, 0.0645 $Å^{-1}$ for Al-SBA-15, 0.0620 $Å^{-1}$ for Ti-SBA-15 and 0.0591 $Å^{-1}$ for Zr-SBA-15. These values correspond to the *d*-spacings with the values d = 95.5 Å for SBA-15, d = 97.3 Å for Al-SBA-15, d = 101.3 Å for Ti-SBA-15 and d = 106.3 Å for Zr-SBA-15. The unit cell parameter, calculated from the (10) diffraction peak using the equation $a = 2 * d_{10} / \sqrt{3}$ was 110 Å for pure SBA-15 silica sample, 112 Å for sample Al-SBA-15, 117 Å for the sample Ti-SBA-15 and 123 Å for the sample Zr-SBA-15. The change in the unit cell parameter reflects the size of the heteroatom incorporated into SBA-15. The different sizes of $[MO_4]$ tetrahedral units, caused by increasing M–O bond lengths in order Si < Al < Ti < Zr, led to the increase of unit cell parameter of hexagonal mesoporous structure. Figure 3b shows change of

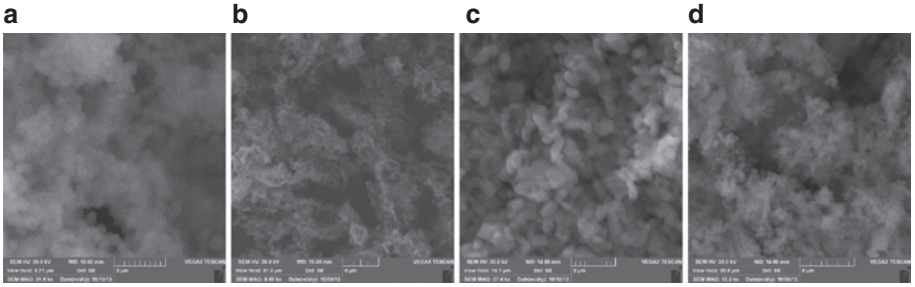

Fig. 2: SEM images of SBA-15 (a), Al-SBA15 (b), Ti-SBA15 (c), Zr-SBA15 (d).

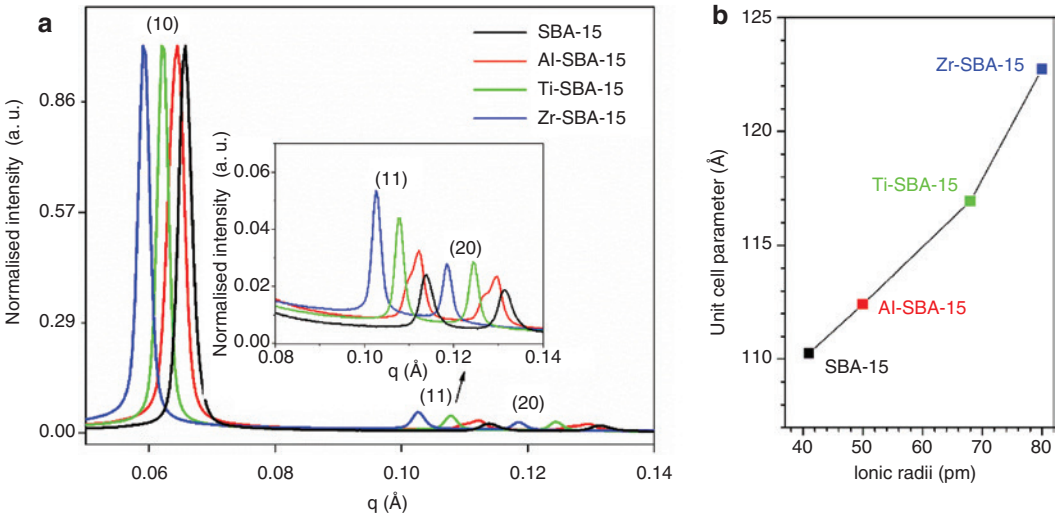

Fig. 3: (a) SAXS patterns of the SBA-15 silica and the samples M-SBA-15 (M = Al, Ti, Zr). (b) Dependence of unit cell parameter on ionic radii of atom M (M = Si, Al, Ti, Zr).

unit cell parameter with change of ionic radius of the metal ion. It is obvious, that nearly linear increase of unit cell parameter was observed, which confirms, that metal ions were successfully incorporated into the mesoporous structure.

Nitrogen adsorption/desorption

Nitrogen adsorption/desorption isotherms of studied samples are present in Fig. 4a. The isotherms are of IV type with H1 hysteresis loop according to IUPAC classification [21]. The initial part of the adsorption isotherms corresponds to adsorption in the micropores and formation of the multilayer film on the pore walls. The isotherms shows a well-defined adsorption/desorption step between partial pressures P/P_0 of 0.66–0.78 for the sample SBA-15, $P/P_0 = 0.70–0.83$ for the sample Al-SBA-15, $P/P_0 = 0.71–0.85$ for the sample Ti-SBA-15 and $P/P_0 = 0.73–0.88$ for the sample Zr-SBA-15, indicative of the filling of mesopores. The shift of the mesopore filling step to higher pressures from the sample SBA-15 to the sample Zr-SBA-15 indicates increase of the pore size.

Desorption from the samples is delayed in comparison with the adsorption and the evaporation step occurs in the range of $P/P_0 = 0.69–0.55$ for the sample SBA-15, $P/P_0 = 0.72–0.60$ for the sample Al-SBA-15, $P/P_0 = 0.74–0.60$ for the sample Ti-SBA-15 and $P/P_0 = 0.75–0.61$ for the sample Zr-SBA-15.

From the adsorption–desorption curves, *t*-plots (the statistical film thickness) were estimated. Figure 4b shows the *t*-plots obtained from the nitrogen sorption measurements in the region from t = 3, 5–8 Å. The intercept of the fitted *t*-plots reflects the amount of microporosity in the studied materials. The value of the intercept is lowest for Zr-SBA-15 silica and highest for pure siliceous SBA-15. The results from the *t*-plot agree very well with micropore surface area and pore size distribution of the samples. The values are summarized in Table 1.

The specific surface area, S_{BET}, was estimated using the Brunauer-Emmett-Teller (BET) equation in a pressure range 0.05–0.30, pore size distribution was calculated using the NLDFT as well as BJH method. The textural properties are summarized in Table 1. It can be seen, that modification of SBA-15 with metal ions led to the decrease of the surface area from 947 m^2/g for SBA-15 to 732 m^2/g for Al-SBA-15, 807 m^2/g for Ti-SBA-15 and 657 m^2/g for Zr-SBA-15. On the other hand, the modification led to the increase of pore size.

In Table 1, the pore sizes of the samples determined by NLFDT and BJH methods are presented. The pore sizes, as determined by both methods, differ by 4–17 Å. It was well documented, that the Kelvin equation based procedures, such as the BJH method, significantly underestimate (~20–30 %) the pore size for

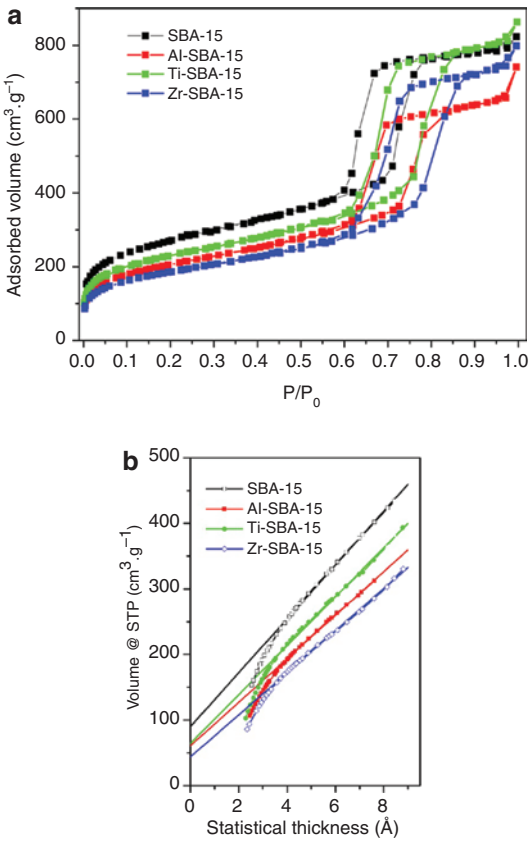

Fig. 4: (a) Nitrogen adsorption/desorption isotherms, (b) *t*-plot curves for the studied samples.

Table 1: Textural properties of the prepared materials.

Sample	S_{BET} (m^2/g)	S_{mic} (m^2/g)	S_{mes} (m^2/g)	S_{ext} (m^2/g)	Mesopore size (Å)		V_{tot} (cm^3/g)	V_{mic} (cm^3/g)	V_{mes} (cm^3/g)
					DFT	BJH			
SBA-15	947	308	583	56	76	72	1.127	0.137	0.990
Al-SBA-15	732	208	435	89	92	84	0.864	0.088	0.776
Ti-SBA-15	807	239	490	78	93	84	1.121	0.105	1.016
Zr-SBA-15	657	156	409	92	111	94	1.011	0.071	0.940

S_{BET}, specific surface area; S_{mic}, surface area of micropores; S_{mes}, surface area of mesopores; S_{ext}, external surface area; V_{tot}, total pore volume; V_{mic}, microporous pore volume; V_{mes}, mesoporous pore volume.

mesopores with < ~10 nm [21] and NLDFT, implemented in commercially available software, provides a reasonably reliable assessment of the pore size distribution for both, micro- and mesopores. Thus, the values in Table 1 determined by NLDFT method should be decisive.

Carbon dioxide and methane adsorption

Single-gas carbon dioxide and methane adsorption isotherms measured at 303 K and up to 20 bar are presented in Fig. 5. The CO_2 adsorption isotherms are virtually Henry-type for all considered samples and thus consistent with moderate gas–solid interactions. At low pressures, below 1 bar, the heteroatoms give only a minor contribution to carbon dioxide adsorption and no significant difference in adsorption between the

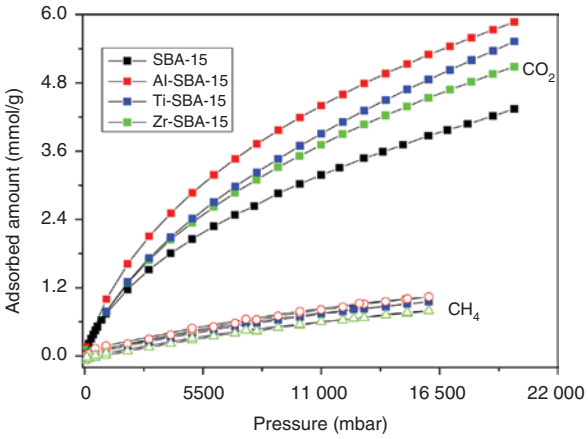

Fig. 5: Carbon dioxide and methane adsorption over studied metal doped samples.

studied samples was observed. The adsorption capacity at 1 bar was in the range 0.74–0.78 mmol/g. At higher pressures the difference between the samples was observed. The highest carbon dioxide adsorption capacity was observed for the sample Al-SBA-15 (5.91 mmol · g^{-1}), followed by the sample Ti-SBA-15 (5.52 mmol · g^{-1}) and sample Zr-SBA-15 (5.07 mmol · g^{-1}). The lowest adsorption capacity was observed for pure siliceous sample SBA-15 (4.34 mmol · g^{-1}). At the maximal experimental pressure no of the measured isotherms reached plateau, what indicates, that the mesopores are still not filled at the maximal pressures. Moreover, the samples differ in the surface area and we have to have in mind, that the textural properties of the samples play relevant role at the adsorption process. Therefore when we normalized adsorption capacity to surface area, the highest adsorption capacity per square meter shows Zr-SBA-15 silica (8.16×10^{-3} mmol · m^{-2}) followed by Al-SBA-15 silica (7.83×10^{-3} mmol · m^{-2}), Ti-SBA-15 silica (6.13×10^{-3} mmol · m^{-2}) and purely siliceous sample SBA-15 silica (4.46×10^{-3} mmol · m^{-2}). These data well documented the influence of metal ions on the adsorption capacity.

In addition to carbon dioxide, we have also studied the adsorption of methane. Carbon dioxide adsorption capacity is markedly higher than methane and depends on samples composition and textural characteristics. One factor influencing the lower CH_4 adsorption is its zero quadruple moment [22] in comparison to permanent electric quadrupole moment of carbon dioxide. The interaction of the carbon dioxide with the metal centers in the silica structure is stronger, in comparison with methane, leading to the higher adsorption. Moreover, the preferential carbon dioxide adsorption at high pressures can be explained by the fact, that adsorption of carbon dioxide at 303 K is about at its critical temperature (T_C), while methane is far above. At 303 K carbon dioxide condensation inside adsorbent pores is possible while methane not. Studies describing carbon dioxide multilayer adsorption at temperatures around critical (even slightly higher) and high pressures confirm this hypothesis [23–25].

Conclusions

Mesoporous silica samples modified by Al^{3+}, Ti^{4+} and Zr^{4+} metal cations were prepared. All samples show regular periodic hexagonal nanoporous structure. Successful incorporation of metals into SBA-15 structure was confirmed by chemical analysis and by increase of unit cell parameter of the hexagonal mesostructure as a function of metal radius, as determined from SAXS patterns. The samples showed apparently higher adsorption capacity to carbon dioxide than to methane, which can be a consequence of higher quadruple moment of carbon dioxide and its stronger interaction with metal cations on the surface of silica. Carbon dioxide adsorption capacity at high pressures was shown to be dependent on the nature of metal cation.

Acknowledgments: This work was supported by the Slovak Research and Development Agency under the contract APVV-15-0520, by the VEGA project no. 1/0745/17 and projects NanoCEXmat I (ITMS No: 26220120019) and NanoCEXmat II (ITMS No. 26220120035), which are supported by the Operational Program "Research and Development" financed through European Regional Development Fund. V.Z. thanks Desy, Hasylab, Hamburg Germany for the support during synchrotron related measurements.

References

[1] J. S. Beck, J. C. Vartuli, W. J. Roth, M. E. Leonowicz, C. T. Kresge, K. D. Schmitt, C. T. W. Chu, D. H. Olson, E. W. Sheppard, S. B. McCullen, J. B. Higgins, J. L. Schlenker. *J. Am. Chem. Soc.* **114**, 10834 (1992).
[2] T.-L. Chew, A. L. Ahmad, S. Bhatia. *Adv. Colloid Interface Sci.* **153**, 43 (2010).
[3] D. Zhao, Q. Huo, J. Feng, B. F. Chmelka, G. D. Stucky. *J. Am. Chem. Soc.* **120**, 6024 (1998).
[4] D. Fuentes-Perujo, J. Santamaría-González, J. Mérida-Robles, E. Rodríguez-Castellón, A. Jiménez-López, P. Maireles-Torres, R. Moreno-Tost, R. Mariscal. *J. Solid State Chem.* **179**, 2182 (2006).
[5] K. Szczodrowski, B. Prélot, S. Lantenois, J.-M. Douillard, J. Zajac. *Micropor. Mesopor. Mater.* **124**, 84 (2009).
[6] Y. Han, D. Zhang. *Curr. Opin. Chem. Eng.* **1**, 129 (2012).
[7] S. Lin, L. Shi, H. Zhang, N. Zhang, X. Yi, A. Zheng, X. Li. *Micropor. Mesopor. Mater.* **184**, 151 (2014).
[8] C. He, B. Tian, J. Zhang. *Micropor. Mesopor. Mater.* **126**, 50 (2009).
[9] Y. J. Acosta-Silva, R. Nava, V. Hernandez-Morales, S. A. Macias-Sanchez, M. L. Gomez-Herrera, B. Pawelec. *Appl. Catal. B Environ.* **110**, 108 (2011).
[10] C. Liang, M.-C. Wei, H.-H. Tseng, E.-C. Shu. *Chem. Eng. J.* **223**, 785 (2013).
[11] K. C. Mouli, S. Mohanty, Y. Hu, A. Dalai, J. Adjaye. *Catal. Today* **207**, 133 (2013).
[12] S.-Y. Chen, T. Mochizuki, Y. Abe, M. Toba, Y. Yoshimura. *Catal. Commun.* **41**, 136 (2013).
[13] J. Iglesias, J. A. Melero, L. F. Bautista, G. Morales, R. Sanchez-Vazquez, M. T. Andreola, A. Lizarraga-Fernandez. *Catal. Today* **167**, 46 (2010).
[14] J. A. Melero, L. F. Bautista, J. Iglesias, G. Morales, R. Sanchez-Vazquez. *Catal. Today* **195**, 44 (2012).
[15] Y. Han, H. Kim, J. Park, S.-H. Lee, J.-Y. Kim. *Int. J. Hydrogen Energy* **37**, 14240 (2012).
[16] A. Zukal, J. Mayerová, J. Čejka. *Phys. Chem. Chem. Phys.* **12**, 5240 (2010).
[17] H. L. Zhao, Z. J. Bian, J. H. Zhou, J. Hu, H. L. Liu. *Scientia Sinica Chim.* **42**, 313 (2012).
[18] V. Zeleňák, D. Halamová, L. Gaberová, E. Bloch, P. Llewelyn. *Micropor. Mesopor. Mater.* **116**, 358 (2008).
[19] M. Badaničová, V. Zeleňák. *Monatshefte fur Chemie* **141**, 677 (2010).
[20] V. Zeleňák, M. Badaničová, D. Halamová, J. Čejka, A. Zukal, N. Murafa, G. Goerigk. *Chem. Eng. J.* **144**, 336 (2008).
[21] M. Thommes, K. Kaneko, A. V. Neimark, J. P. Olivier, F. Rodriguez-Reinoso, J. Rouquerol, K.S.W. Sing. *Pure Appl. Chem.* **87**, 1051 (2015).
[22] G. Sethia, R. S. Somani, H. Ch. Bajaj. *RSC Adv.* **5**, 12773 (2015).
[23] G. Bellussi, P. Broccia, A. Carati, R. Millini, P. Pollesel, C. Rizzo, M. Tagliabue. *Micropor. Mesopor. Mater.* **146**, 134 (2011).
[24] M. S. Schneider, J. D. Grunwaldt, A. Baiker. *Langmuir* **20**, 2890 (2004).
[25] L. Zhou, S. Bai, W. Su, J. Yang, Y. Zhou. *Langmuir* **19**, 2683 (2003).